Magnetic structure of Dy^{3+} in hexagonal multiferroic $DyMnO_3$

S. Nandi,[1,2] A. Kreyssig,[1,2] J. Q. Yan,[1,2] M. D. Vannette,[1,2] J. C. Lang,[3] L. Tan,[1,2] J. W. Kim,[1,2] R. Prozorov,[1,2] T. A. Lograsso,[1] R. J. McQueeney,[1,2] and A. I. Goldman[1,2]

[1]*Ames Laboratory, U.S. DOE, Ames, Iowa 50011, USA*

[2]*Department of Physics and Astronomy, Iowa State University, Ames, Iowa 50011, USA*

[3]*Advanced Photon Source, Argonne National Laboratory, Argonne, Illinois 60439, USA*

(Received 25 June 2008; published 22 August 2008)

Element specific x-ray resonant magnetic scattering (XRMS) investigations were undertaken to determine the magnetic structure of the multiferroic compound, hexagonal $DyMnO_3$. In the temperature range from 68 K down to 8 K the Dy^{3+} moments are aligned and antiferromagnetically correlated in the **c** direction according to the magnetic representation Γ_3. The temperature dependence of the observed intensity can be modeled assuming the splitting of ground-state doublet crystal-field levels of Dy^{3+} by the exchange field of Mn^{3+}. XRMS together with magnetization measurements indicate that the magnetic representation is Γ_2 below 8 K.

DOI: 10.1103/PhysRevB.78.075118 PACS number(s): 75.25.+z, 75.50.Ee, 75.80.+q, 77.80.−e

Magnetoelectric multiferroics—systems that exhibit both ferroelectricity and magnetism in the same phase—have attracted renewed attention in the last few years.[1] Understanding the interplay between both phenomena may open up device paradigms—such as electric-field controlled magnetic data storage. Strong coupling between magnetic and ferroelectric order has been recently observed in rare-earth (R) manganites such as hexagonal $RMnO_3$,[2,3] orthorhombic $RMnO_3$,[4] RMn_2O_5,[5] and other compounds. $DyMnO_3$ is generally found in orthorhombic form but under special conditions the hexagonal phase may be stabilized.[6,7] $DyMnO_3$, then sits at the boundary between the orthorhombic and hexagonal multiferroic manganates.

Hexagonal $DyMnO_3$ shows ferroelectricity at room temperature[6] and it was concluded from magnetization measurements that the Dy^{3+} moments order ferrimagnetically below 7 K. Nevertheless, the magnetic structure and the corresponding magnetic symmetry remained unknown.[7] Since magnetic structure determination is a prerequisite for understanding the coupling between ferroelectricity and magnetism and it was shown for hexagonal $HoMnO_3$ (Ref. 2) and orthorhombic $DyMnO_3$ (Ref. 8) that the rare-earth magnetic ordering plays a very important role in the magnetoelectric coupling, it is important to know the details of the magnetic ordering of the Dy^{3+} moments. As the naturally occurring isotope of Dy is highly neutron absorbing, the magnetic structure determination by neutron diffraction is challenging and has not, to date, been done. In addition, discriminating between the two magnetic sublattices, Dy^{3+} and Mn^{3+}, is very difficult. An x-ray resonant magnetic scattering (XRMS) study of $DyMnO_3$ is complementary to neutron measurements but is more direct in determining the magnetic structure associated with, and the order parameter of the Dy^{3+} moments.

Single crystals of $DyMnO_3$ were grown using a floating zone method.[7] For the XRMS measurements, a piece of an as-grown single crystal of approximate dimensions $4\times3\times1$ mm^3 was selected. The surface of the crystal was nearly perpendicular to the **c** axis. The XRMS experiment was performed on the 6ID-B beamline at the Advanced Photon Source at the Dy L_{III} absorption edge (E=7.790 keV). The incident radiation was linearly polarized perpendicular to the vertical scattering plane (σ polarized) with a spatial cross section of 0.6 mm (horizontal) $\times$ 0.2 mm (vertical). In this configuration, resonant magnetic scattering rotates the plane of linear polarization into the scattering plane (π polarization). In contrast, charge scattering does not change the polarization of the scattered photons (σ-σ scattering). Pyrolytic graphite (PG) (0 0 6) was used as a polarization analyzer to suppress the charge and fluorescence background relative to the magnetic scattering signal. For measurements of the (0 0 l) and (0 h l) magnetic reflections, with l odd, the sample was mounted at the end of the cold finger of a displex cryogenic refrigerator with the reciprocal $\mathbf{b}^\star$-$\mathbf{c}^\star$ plane coincident with the scattering plane. Although these reflections are forbidden for charge reflections, they can be strongly contaminated by multiple charge scattering. However, we were able to minimize multiple-scattering contribution at the resonant energy through a judicious choice of the azimuth angle.

Figure 1 shows the magnetization curves and magnetic susceptibility of a $DyMnO_3$ single crystal, measured using a quantum design superconducting quantum interference device (SQUID) magnetometer. In the inset to Fig. 1(c), we see a kink in magnetic susceptibility at 68 K, signaling the onset of magnetic order. At approximately 8 K, there is a dramatic change in the magnetic susceptibility, indicating a phase transition from the intermediate-temperature phase, ITP (68–8 K) to the low-temperature phase, LTP (below 8 K).

In the ITP, magnetic intensity was found at the (0 0 9) reciprocal lattice point, which is nominally forbidden for charge scattering. To confirm the resonant behavior of this feature, we performed energy scans (as shown in Fig. 2) through the Dy L_{III} absorption from 3 to 75 K and observed one predominant resonance peak, approximately 6 eV above the absorption edge. This peak arises from dipole resonant scattering involving an intermediate-state transition between the core $2p$ and the empty $5d$ states.[10] We also note the presence of a weak quadrupole resonance ($2p$ to $4f$ states) at approximately 5 eV below the absorption edge. In the energy scans, no resonance intensity was observed above the ITP. Furthermore from Fig. 2, we see that the dipole resonance intensity increases with decreasing temperatures in the ITP. However, this signal disappears abruptly below 8 K.

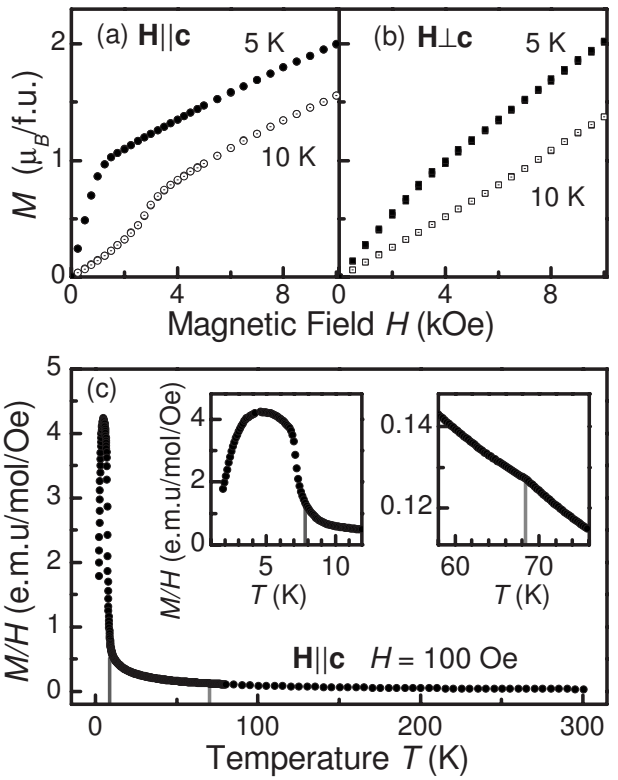

FIG. 1. [(a)-(b)] Magnetization curves of the $DyMnO_3$ single crystal measured along and perpendicular to the **c** direction at 5 and 10 K. (c) Temperature dependence of magnetic susceptibility was measured on heating of the zero-field cooled sample in a field of 100 Oe applied parallel to the **c** axes. The insets show details of the magnetic susceptibility near the transition temperatures of the order of Dy^{3+} moments. Marked vertical lines are the transition temperatures determined from the XRMS measurements.

Generally, the local sample heating by the intense incident undulator beam is very strong for insulating materials such as $DyMnO_3$, particularly at low temperatures. Therefore, to characterize the beam heating effect and to determine the transition temperature for magnetic ordering of Dy^{3+}, we measured the dipole resonance intensity of the (0 0 9) reflection with different attenuators as shown in the inset to Fig. 3. Since the normalized peak intensity and transition temperature remain nearly the same using attenuators with transmissions of $t \sim 7\%$ and $\sim 1\%$, temperature-dependent measurements were performed with the former. Figure 3 shows the temperature dependence of the integrated intensity for the (0 0 9) reflection, determined by fitting θ scans (rocking curves) with a Lorentzian function. Below 68 K, the dipole intensity increases gradually with decreasing temperature. The temperature of the onset of the magnetic order of Dy^{3+} agrees well with the kink in magnetization data from the same sample as shown in Fig. 1. Again from Fig. 3, we see that the magnetic intensity of the (0 0 9) reflection decreases rapidly and goes to zero below 8 K, signifying the phase transition to LTP.

We now turn to the analysis of the magnetic structure in the ITP. In order to determine the magnetic representation we must look into the details of six magnetic representations that are possible for the crystallographic space group $P6_3cm$ and

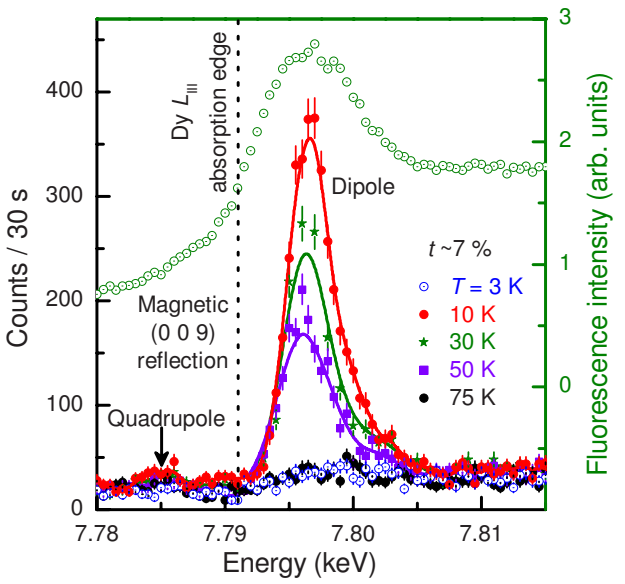

FIG. 2. (Color online) Energy scans of the (0 0 9) reflection and of the fluorescence signal. The small peak marked by the vertical arrow indicates weak quadrupole resonance. The dashed line depicts the Dy L_{III} absorption edge as determined from the inflection point of the fluorescence signal. The solid lines are guide to the eye.

are listed in the Table I. The observation of nonzero intensity for the (0 0 9) reflection clearly excludes the magnetic representations Γ_1, Γ_2, Γ_4, and Γ_5 for the magnetic order of Dy^{3+} (see Table I) because only the representations Γ_3 and Γ_6 yield nonzero intensity for (0 0 l) reflections with l odd. The Dy^{3+} moments are aligned in the hexagonal **c** direction according to representation Γ_3, whereas they are aligned in the **a**-**b** plane in representation Γ_6.

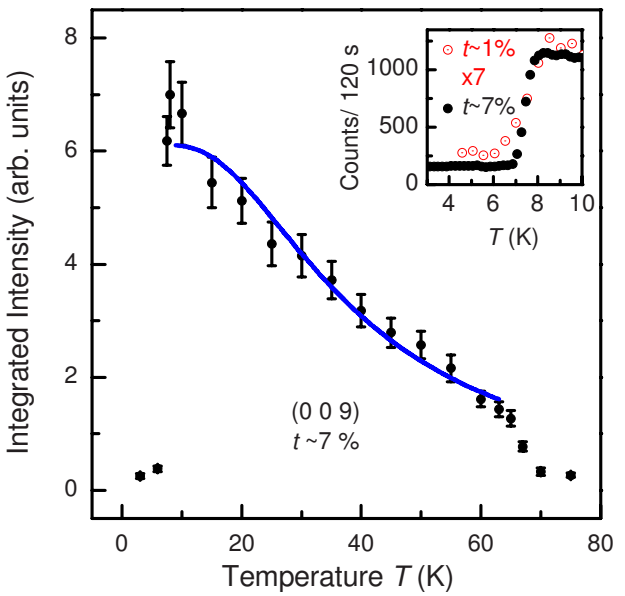

FIG. 3. (Color online) Temperature dependence of the integrated intensity of the dipole resonance for the (0 0 9) reflection. The inset shows details of the low-temperature phase transition. The solid blue line is a fit to the data in the intermediate magnetic phase by a model as described in the text.

TABLE I. The six possible magnetic representations and the corresponding basis vectors of the crystallographic space group $P6_3cm$ associated with a magnetic unit cell, same as the crystallographic unit cell (Ref. 9). The atomic positions for Dy are given in brackets. $[z,+,-]$ depict $z_{2a}=0.277, +\mu^c_{2a}, -\mu^c_{2a}$, and $z_{4b}=0.237, +\mu^c_{4b}, -\mu^c_{4b}$ for the Wyckoff sites Dy($2a$) and Dy($4b$), respectively (Ref. 6). The symbol [0] labels no ordered magnetic moment at this site. The directions of magnetic moments for the Γ_5 and Γ_6 magnetic representations are denoted by $[\mathbf{e}_x,\mathbf{e}_y,\mathbf{e}_z]$, where $\mathbf{e}_x$ and $\mathbf{e}_y$ are in the basal plane forming a 120 angle between them and the $\mathbf{e}_z$ vector is parallel to the sixfold axis. The condition for a particular reflection is determined for the present experimental geometry and a dipole XRMS signal.

Magnetic representation	Dy($2a$) $\begin{pmatrix}0\\0\\z\end{pmatrix}$	$\begin{pmatrix}0\\0\\z+\frac{1}{2}\end{pmatrix}$	Dy($4b$) $\begin{pmatrix}\frac{1}{3}\\\frac{2}{3}\\z\end{pmatrix}$	$\begin{pmatrix}\frac{2}{3}\\\frac{1}{3}\\z\end{pmatrix}$	$\begin{pmatrix}\frac{1}{3}\\\frac{2}{3}\\z+\frac{1}{2}\end{pmatrix}$	$\begin{pmatrix}\frac{2}{3}\\\frac{1}{3}\\z+\frac{1}{2}\end{pmatrix}$	Magnetic reflection $(0\ 0\ l)$ l odd	$(0\ h\ l)$ l odd
				Moments in **c** direction				
$\Gamma_1 \equiv P6_3cm$	0	0	+	−	−	+	No	Yes
$\Gamma_2 \equiv P6_3c'm'$	+	+	+	+	+	+	No	No
$\Gamma_3 \equiv P6'_3cm'$	+	−	+	+	−	−	Yes	Yes
$\Gamma_4 \equiv P6'_3c'm$	0	0	+	−	+	−	No	No
				Moments in **a**-**b** plane				
$\Gamma_5(P6'_3)$	$[u\ v\ 0]$	$[u\ v\ 0]$	$[p\ q\ 0]$	$[r\ s\ 0]$	$[r\ s\ 0]$	$[p\ q\ 0]$	No	No iff $p=r$ and $q=s$
$\Gamma_6(P6_3)$	$[u\ v\ 0]$	$[\bar{u}\ \bar{v}\ 0]$	$[p\ q\ 0]$	$[r\ s\ 0]$	$[\bar{r}\ \bar{s}\ 0]$	$[\bar{p}\ \bar{q}\ 0]$	Yes	Yes

We measured the off-specular reflections (0 3 9) and (0 $\bar{3}$ 9) to determine the moment direction. The structure factor is the same for both reflections, but the dipole scattering cross section is different providing strong sensitivity to the moment direction. For our scattering geometry, the dipole scattering amplitude $f \propto \vec{k}' \cdot \vec{\mu}$,[11] where $\vec{k}'$ and $\vec{\mu}$ are the wave vector of the scattered photons and the magnetic moment, respectively. For moments aligned along the **c** direction (Γ_3), the magnetic intensity $I \propto \sin^2(\theta \pm \alpha)$; for moments in the **a**-**b** plane (Γ_6) $I \propto \cos^2(\theta \pm \alpha)$, where θ is the Bragg angle and α is the angle that the scattering vector **Q** makes with the crystallographic **c** direction perpendicular to the surface of the sample. The '+'/'−' signs are for larger/smaller angles for the outgoing beam with respect to the sample surface. The calculated ratio $I(0\ 3\ 9)/I(0\ \bar{3}\ 9)=65$ and 0.02 are for moments along the **c** direction and in the **a**-**b** plane, respectively. Since the absorption is different for these two off-specular reflections, proper normalization using the closest charge reflections was performed to determine the experimental ratio of 80 ± 20. Thus, within experimental error, the magnetic moments are primarily aligned in the hexagonal **c** direction and the Dy^{3+} moments order according to the magnetic representation Γ_3 in the ITP.

Figure 3 shows a gradual increase in the observed intensity as the temperature is decreased in the ITP. With reference to other systems, such as Nd_2BaNiO_5 and Nd_2CuO_4, the temperature dependence of the integrated intensity in the ITP can be explained with a ground-state doublet crystal-field level, split by an exchange field.[12–14] The Kramer's Dy^{3+} ions in $DyMnO_3$ are at the positions of trigonal symmetry and, therefore, must have a doublet ground state.[15,16] At low temperatures only the ground-state doublet is appreciably populated because the energy difference between the ground-state and the next crystal electric-field levels, in general, is large.[16] Taking into account only the ground-state doublet and a splitting, $\Delta(T)$, we can write[12,14]

$$I(T) = I(0)\left[\tanh\frac{\Delta(T)}{2kT}\right]^2, \tag{1}$$

where $I(T)$ and $I(0)$ are the intensities at the temperature T and 0 K, respectively. For an exchange field produced by the ordering of the Mn^{3+} sublattice, the doublet splitting, $\Delta(T)$, is proportional to the ordered magnetic moment of Mn^{3+}.[12] In the case of $DyMnO_3$, however, the ordering temperature and the temperature dependence of Mn^{3+} moments have not been determined. For the nearest hexagonal compound, $HoMnO_3$, the Mn^{3+} moments order below 76 K and saturate within a few Kelvin.[17] Anticipating a similar behavior for the Mn^{3+} moments in $DyMnO_3$, we assumed $\Delta(T)$ to be constant in the temperature range of fitting, 10–62 K. The fitting yields $\Delta = (5.8 \pm 0.8)$ meV. Thus, the temperature dependence of integrated intensity in the ITP can be modeled using a simplified picture of the crystal-field splitting and suggests an induced magnetic order of Dy^{3+} in this ITP. This analysis also predicts that the Mn^{3+} moments in $DyMnO_3$ order according to Γ_3 representation in the ITP. Neutron-scattering measurements to confirm this prediction are planned.

We now turn to the investigation of the magnetic structure in the LTP, where the magnetic intensity of the (0 0 9) reflection goes to zero (see Fig. 3). Referring again to Table I, we can readily exclude the magnetic representations Γ_3 and Γ_6 as these reflections should yield finite intensity. The intensity of the (0 1 9) reflection also goes to zero, as shown in Fig. 4. This excludes the magnetic representation Γ_1 for the LTP as the intensity of this reflection should be finite but large compared to ITP.[18] Therefore, the remaining possible magnetic representations are Γ_2, Γ_4, and Γ_5. These representations yield intensity at the charge allowed reciprocal lattice points (l even). Since the magnetic signal is weak compared to the charge scattering, separation of a magnetic signal from the charge signal is extremely difficult in an XRMS

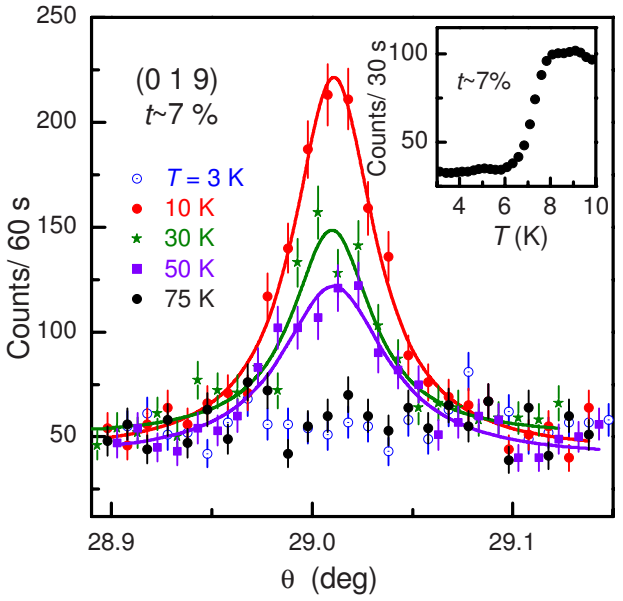

FIG. 4. (Color online) Representative rocking scans for an off-specular reflection (0 1 9). The inset shows the details of the low-temperature phase transition. The peak intensity was measured to characterize the transition temperature. Lines are guide to the eye.

experiment.[19] However, we note that while Γ_4 is antiferromagnetic along the **c** direction, the representations Γ_2 and Γ_5 correspond to ferromagnetic moments along the **c** direction and in the **a**-**b** plane, respectively. Figures 1(a) and 1(b) show the magnetization measurement along and perpendicular to the **c** direction at 5 (LTP) and 10 K (ITP). A steep rise to a sharp kink in the magnetization in the LTP for small fields ($\leq$1 kOe) along the **c** direction indicates a ferromagnetic moment along this direction, consistent with the reported results of Ivanov *et al.*[7] Therefore, magnetization together with XRMS measurements suggest that Γ_2 is the magnetic representation in the LTP. According to this representation the Dy^{3+} moments at each site are ferromagnetically aligned but the correlation between them can be parallel (ferromagnetic) or antiparallel (ferrimagnetic). As the uncompensated magnetic moment along the **c** direction, determined from the extrapolation of high-field magnetization data to zero field, is only $\sim 1\mu_B$ per formula unit, much less than the free magnetic moment (10.6 μ_B) of Dy^{3+}, a ferrimagnetic alignment of Dy^{3+} moments is expected.

In summary, we have determined the magnetic structure of Dy^{3+} moments in $DyMnO_3$ to be Γ_3 in the ITP (between 68 and 8 K). The Dy^{3+} moments are aligned and antiferromagnetically correlated along the **c** direction. The temperature dependence of the magnetic intensity in the ITP can be explained by assuming a splitting of the ground-state doublet by the exchange field from the ordered Mn^{3+} moments. In the LTP (below 8 K), XRMS, together with magnetization measurements, indicates that Γ_2 is the magnetic representation and the Dy^{3+} moments are ferrimagnetically aligned in the hexagonal **c** direction. We note that the magnetic structure in $DyMnO_3$ is the same as in $HoMnO_3$ in the ITP. However, in the LTP the magnetic order is different: the Ho^{3+} moments are antiferromagnetically aligned according to Γ_1 in contrast to the ferrimagnetic alignment of the Dy^{3+} moments in $DyMnO_3$. It is likely that the striking difference is due to the complex interplay between the magnetism of the two sublattices, Dy^{3+}/Ho^{3+} and Mn^{3+}.

We appreciate the help of Daniel Haskel for additional measurements. We are indebted to D. S. Robinson for his help during the experiments. The work at the Ames Laboratory and at the MU-CAT sector was supported by the U.S. DOE under Contract No. DE-AC02-07CH11358. The use of the Advanced Photon Source was supported by U.S. DOE under Contract No. DE-AC02-06CH11357.

[1] N. A. Spaldin and M. Fiebig, Science **309**, 391 (2005).
[2] F. Yen, C. R. dela Cruz, B. Lorenz, Y. Y. Sun, Y. Q. Wang, M. M. Gospodinov, and C. W. Chu, Phys. Rev. B **71**, 180407(R) (2005).
[3] B. Lorenz, F. Yen, M. M. Gospodinov, and C. W. Chu, Phys. Rev. B **71**, 014438 (2005).
[4] T. Kimura, T. Goto, H. Shintani, K. Ishizaka, T. Arima, and Y. Tokura, Nature (London) **426**, 55 (2003).
[5] N. Hur, S. Park, P. A. Sharma, J. S. Ahn, S. Guha, and S.-W. Cheong, Nature (London) **429**, 392 (2004).
[6] N. Kamegashira, H. Satoh, and S. Ashizuka, Mater. Sci. Forum **449-452**, 1045 (2004).
[7] V. Y. Ivanov, A. A. Mukhin, A. S. Prokhorov, A. M. Balbashov, and L. D. Iskhakova, Phys. Solid State **48**, 1726 (2006).
[8] O. Prokhnenko, R. Feyerherm, E. Dudzik, S. Landsgesell, N. Aliouane, L. C. Chapon, and D. N. Argyriou, Phys. Rev. Lett. **98**, 057206 (2007).
[9] A. Muñoz, J. A. Alonso, M. J. Martínez-Lope, M. T. Casáis, J. L. Martínez, and M. T. Fernández-Díaz, Chem. Mater. **13**, 1497 (2001).
[10] J. P. Hannon, G. T. Trammell, M. Blume, and D. Gibbs, Phys. Rev. Lett. **61**, 1245 (1988).
[11] J. P. Hill and D. F. McMorrow, Acta Crystallogr., Sect. A: Found. Crystallogr. **52**, 236 (1996).
[12] M. N. Popova, S. A. Klimin, E. P. Chukalina, E. A. Romanov, B. Z. Malkin, E. Antic-Fidancev, B. V. Mill, and G. Dhalenne, Phys. Rev. B **71**, 024414 (2005).
[13] A. Zheludev, J. P. Hill, and D. J. Buttrey, Phys. Rev. B **54**, 7216 (1996).
[14] R. Sachidanandam, T. Yildirim, A. B. Harris, A. Aharony, and O. Entin-Wohlman, Phys. Rev. B **56**, 260 (1997).
[15] B. G. Wybourne, *Spectroscopic Properties of Rare Earths* (Interscience, New York, 1965).
[16] D. Bravo, A. A. Kaminskii, and F. J. López, J. Phys.: Condens. Matter **10**, 3261 (1998).

[17] T. Lonkai, D. Hohlwein, J. Ihringer, and W. Prandl, Appl. Phys. A: Mater. Sci. Process. **74**, S843 (2002).
[18] S. Nandi, A. Kreyssig, L. Tan, J. W. Kim, J. Q. Yan, J. C. Lang, D. Haskel, R. J. McQueeney, and A. I. Goldman, Phys. Rev. Lett. **100**, 217201 (2008).
[19] J. W. Kim, A. Kreyssig, P. Ryan, E. Mun, P. C. Canfield, and A. I. Goldman, Appl. Phys. Lett. **90**, 202501 (2007).